Early-mid Miocene erosion rates inferred from

Hazeva River fluvial chert pebbles using cosm

Michal Ben-Israel[1], Ari Matmon[1], Alan J. Hidy[2], Yoav Avni[3], Greg B

[1]*The Institute of Earth Sciences, Hebrew University of Jerusalem, Jerusalem, 91904*

[2]*Center for Accelerator Mass Spectrometry, Lawrence Livermore National Laborat*

[3]*Geological Survey of Israel, Yesha'yahu Leibowitz 32, Jerusalem, 96921 Israel*

[4]Berkeley Geochronology Center, Berkeley, California 94709, USA

Correspondence to: Michal Ben-Israel (michal.benisrael@mail.huji.ac.il)

Abstract. In this work, we utilize a novel application of cosmogenic ^{2} to compare exposure times measured in eroding surfaces in the Jord exposure times from chert pebbles transported by the Miocene Hazeva River was a large fluvial system (estimated catchment size >100,000 k Plateau and Sinai Peninsula into the Mediterranean Sea during the established after the rifting of the Red Sea uplifted the Arabian Pla Following late Miocene to early Pliocene subsidence along the Dead Se system was abandoned and dissected, resulting in new drainage divid We find that modern erosion rates derived from cosmogenic ^{21}Ne, ^{26}

in hyperarid environments. Miocene exposure times are shorter even
account for bedrock erosion in addition to maintained transport alo
exposure times in Miocene cherts correspond to faster paleo-erosion ra
combination of continuous surface uplift and significantly wetter cli
early-mid Miocene.

1. Introduction

Tectonic and climatic conditions control geomorphological processes
weathering, and sediment generation and transport (e.g., Allen, 2008;
2012). Changes in rates of continental uplift and climatic conditions co
sediment production, transport, and storage and influence fluvial sy
sediment archives (e.g., DiBiase and Whipple, 2011; Ferrier et al.,
Cosmogenic nuclides, mostly radiogenic ^{26}Al and ^{10}Be, have been
weathering and erosion rates in fluvial systems across different scales a
Bierman, 1994; von Blanckenburg, 2005). The decreased preservation
systems, due to burial or recycling, adds difficulty to the reconstructio
conditions with increased sediment age (e.g., Anderson et al., 1996; Gu
et al., 2002). Furthermore, even when geological circumstances do al
older sediments, rates prior to the Pliocene cannot be quantified wit
cosmogenic radionuclides (^{10}Be and ^{26}Al) due to their half-lives
accordingly; Ivy-Ochs and Kober, 2008). Unlike their radioactive cou

mid Miocene and rates of hyperarid environments eroding today,
influence of the tectonic and climatic conditions that operated in the re

2. Geological Setting

Following an extended period of transgression that ended in the late
Sea retreated to its current location (Garfunkel and Horowitz, 196
tectonic tranquility was followed by a series of tectonic and magmatic
rifting of the Red Sea and the Gulf of Aden in the late Eocene to early O
Bohannon et al., 1989; Bosworth et al., 2005; Omar and Steckler, 19
Myr, regional doming associated with the emergence of the Afar p
Peninsula from near sea level to its present elevation of ~1km (e.g., Fe
et al., 2019; Wilson et al., 2014). As a result of this uplift, widespread
regional truncation surface developed in the northern Red Sea and the
older strata down to Precambrian formations depending on the preexi
2012). Following these events, during the early-mid Miocene, the upl
a newly established fluvial system, termed the Hazeva River, which f
the eroded terrains towards the Mediterranean Sea, and drained an es
(Garfunkel and Horowitz, 1966; Zilberman and Calvo, 2013; Fig. 1).
operated until the subsidence of the Dead Sea Rift, during the late
brought on a dramatic change in morphology, which led to the disrup
system, the last of its kind in the region (Garfunkel, 1981). By the early
drainage systems replaced the Hazeva River, draining the region towar

Arabian Plateau and Sinai and deposited simultaneously by the Haz
Calvo, 2013). The first member is sub-rounded monocrystalline q
Phanerozoic Nubian sandstone, as well as from outcrops of Precambr
Arabian-Nubian shield (Calvo and Bartov, 2001). The second memb
chert pebbles, either interbedded with the quartz sand or forming horiz
sequence (Zilberman and Calvo, 2013). The chert comprising these pe
east of the Dead Sea Rift, and therefore fluvial deposits on the west sid
chert" (Kolodny, 1965) must have been emplaced prior to rifting. The
is constrained by the Karak dike (~20 Myr) which intrudes the lo
formation (Calvo and Bartov, 2001). During the Miocene climatic c
hypothesized to have been wetter (e.g., Kolodny et al., 2009). Curren
middle latitude dry warm desert extending from northern Africa to we
Desert remaining hyperarid at least since the middle Pleistocene (Ami

3. Methodology and Analytical Procedures

3.1 Sampling Strategy

Cosmogenic nuclides in sediments accumulate throughout the sedime
material is exposed during weathering and exposure of the source r
drainage system, and to a much lesser degree following burial at s
destination. Unlike the more commonly used radioactive cosmogenic
substantially or even completely over multiple sedimentary cycles, ^{21}N
the concentration of ^{21}Ne measured in sediments may have accumul

We collected and analyzed ten samples in total, eight Hazeva formati
Jordanian cherts. The Hazeva samples include three samples of quart
115 MHS5), and five individual chert pebbles (MHC2, MHC23, MHC5a
obtained from two Miocene Hazeva exposures (Fig. 2 B-C; Table 1).
collected from deeply shielded locations to minimize the effects of
section 5.1 for further discussion). The quartz sand and the chert pebbl
the Miocene Hazeva system and share a similar exposure history. Ho
120 exposed in previous sedimentary cycles throughout the Mesozoic
accumulated cosmogenic ^{21}Ne. In contrast, the chert was deposite
exposed, transported, and buried during the Miocene (Avni et al., 2
cosmogenic ^{21}Ne measured in the quartz sand represents multipl
cosmogenic ^{21}Ne measured in the chert pebbles represents erosion ar
125 sedimentary cycle in the Miocene Hazeva River. Additionally, two in
chert nodules (EJC3 and EJC5) were collected from exposed bedro
source rock in central Jordan (Fig. 2A). Unlike the Miocene samples,
at least one full sedimentary cycle, the Jordanian chert nodules accum
only during exhumation to the currently exposed surface. Therefor
130 concentrations measured in the Jordanian cherts represent averaged ra
~10^5 yr.

3.2 Preparation of Chert and Quartz Samples and Analytical Proc

Chert pebbles (ranging 4-14 cm, b axis) were crushed, and both chert ar
to 250-850 µm. Chert and quartz samples were processed to separate c

the degassing results with the uncrushed aliquots. Ca. 70 mg from the
mg from the quartz samples were encapsulated in a tantalum packet
using a diode laser micro-furnace at 2-4 heating steps between 450 an
each temperature step. Ne isotope measurements used the BGC "Ohio
described in Balco et al., (2019). 20-30 grams of leached and clea
samples and three chert samples were processed to separate Be and Al
Nishiizumi (1992) and Bierman and Caffee (2001). These were then
$^{26}Al/^{27}Al$ at the Centre for Accelerator Mass Spectrometry, Law
Laboratory, and calibrated against house standards and blanks.

3.3 Cosmogenic Scaling and Correction Factors

Exposure and burial times and erosion rates were calculated based o
using time-independent scaling (Stone, 2000) and production mechan
(2008), given sea-level high-latitude production rates of 4.96 atoms
atoms/g SiO_2/year for ^{26}Al (Balco et al., 2008), and 18.1 atoms/g SiO_2
Luna et al., 2018).

4. Results

4.1 ^{21}Ne in Quartz Sand and Cherts

For the chert samples, <2% of the total ^{21}Ne and no more than 1% of th
released above 950°C (see the Supplementary Tables S1-4). Therefor
performed at 450, 700, and 950°C heating steps for chert samples an
steps for quartz samples (Table 1). Of the total ^{21}Ne measured, >85

^{21}Ne was released in the 950°C step, determining the concentration of
MHC2 is beyond analytical abilities. Therefore, this sample was
calculations, discussion, and interpretations. It is important to note
isotopic values of $^{21}Ne/^{20}Ne$ and $^{22}Ne/^{20}Ne$ ratios at the low-temperatu
cosmogenic component of $^{21}Ne_{ex}$ from the nucleogenic component, p
and Th within the crystal lattice, is not trivial. Nonetheless, as all ch
nodules and Miocene chert pebbles) share the same lithology, any
concentrations must be due to the cosmogenic component.

The chert pebbles and quartz sands sampled at both Miocene H
concentrations of $^{21}Ne_{cos}$ ranging between $0.00\pm1.88\cdot10^{6}$ and 8.89 ± 1.8
At both Miocene Hazeva sites, the cosmogenic ^{21}Ne concentrations m
similar or lower compared to sand samples. These measured con
understanding that the sand samples contain quartz grains that originat
that were deposited throughout the Phanerozoic and could have unde
cycles before they were exhumed and transported by the Miocene fluvia
could also have higher concentrations of nucleogenic ^{21}Ne as the sourc
Ma (Kolodner et al., 2009). Conversely, the Hazeva chert samples ar
young Eocene source rock and were exposed during one sedimentary
samples of Jordanian chert nodules collected from *in situ* Eoce
cosmogenic ^{21}Ne concentrations, higher compared to the Miocene Haz
Diffusion kinetics of Ne in quartz have been examined experimentally
and Farley, 2005; Tremblay et al., 2014) but have yet to be tested o

4.2 ^{10}Be and ^{26}Al in Quartz Sand and Cherts

^{10}Be and ^{26}Al concentrations were measured in three Miocene sand sa
MHS5), the two Eocene chert nodules (EJC3 and EJC5), and two c
MHC6). ^{10}Be results for sample MHC5b and ^{26}Al results for sample MH
1). Miocene sand and chert samples show ^{10}Be and ^{26}Al concentrations
with extended periods of burial ($\leq 0.39.\pm 0.03 \cdot 10^5$ atoms/g SiO_2 for
atoms/g SiO_2 for ^{26}Al). Currently eroding Eocene nodules show higher
^{26}Al, with sample EJC3 showing ^{26}Al/^{10}Be ratio that is consistent wit
and sample EJC5 showing a lower ^{26}Al/^{10}Be ratio, suggesting a more co
(see Discussion section).

5. Discussion

5.1 Correcting for Post-Burial Muonic Produced Cosmogenic ^{21}Ne

When examining concentrations of cosmogenic nuclides in sediment
extended periods, post-burial production needs to be considered. At or
interactions are the main pathway for *in situ* production of cosmogen
>95% for ^{26}Al, ^{10}Be, and ^{21}Ne (Dunai, 2010). However, the relative co
muon interactions increases with burial depth. While production rates
be significant when integrated over long periods, especially for stabl
component does not represent surface processes, and therefore, it is
contribution to the measured cosmogenic component. For radioactive
as ^{10}Be and ^{26}Al, their initial concentrations (acquired during exposur

consists of clastic sediments with a density of ~2 g/cm^3). The discre
burial depth, only tens of meters below the surface, and the deduced bu
of surface erosion that occurred during the last ~2 Myr (Matmon
references therein). Additionally, the relatively large uncertainty on
could account for some of this discrepancy (Balco, 2017; Balco et a
show that the cosmogenic ^{21}Ne produced post-burial over 18 Myr at c
lower than the $^{21}Ne_{ex}$ measured in the presented samples (includin
maximal calculated post-burial cosmogenic ^{21}Ne concentration acc
SiO_2, which is lower than the analytical uncertainty for all measured M
MHC2, where no cosmogenic ^{21}Ne was measured. However, sample
the interpretations of the results. Therefore, we consider post-burial c
to be insignificant for the presented Miocene exposure times.

5.2 Calculating Modern and Miocene Exposure Times

Exposure times at the surface calculated from cosmogenic ^{21}Ne concen
chert nodules from the Jordanian Central Plateau (EJC3 and EJC5) ra
193 kyr and a maximum of 454 kyr (correlating to cosmogen
$8.08\pm1.48\cdot10^6$ and $12.10\pm2.43\cdot10^6$ atoms/g SiO_2).

In comparison to the Jordanian samples, quantifying exposure times
cosmogenic ^{21}Ne concentrations is not trivial, most notably due to the
local cosmogenic production rates. The production rate of cosmogen
altitude as the air pressure and shielding effect of the atmosphere decr
the latitude of the Arabian Peninsula during the early Miocene was sim

Hazeva fluvial system at ~18 Ma. Nevertheless, this stratigraphic
determine whether the Arabian Peninsula reached its current eleva
Miocene or whether additional uplift occurred over the past 20 M
exhumation along the eastern flank of the Dead Sea Rift do not provide
the timing of surface uplift. Surface uplift histories based on cooling a
and river profiles (Wilson et al., 2014), conclude that during the last ~
the Arabian Peninsula was uplifted to its current elevation(Feinstein
2014). However, in a recent work, Morag et al. (2019) present thermoch
apatite (U–Th)/He and fission-track data from a transect across the ea
in SW Sinai. The researchers suggest that uplift and exhumation along
Rift flank slowed substantially post ~18 Ma. This decline reflects a dec
indicate that the Jordanian Plateau has reached close to its current ele
Hazeva River was active. One more approach to evaluate the pale
Jordanian Plateau is to calculate this elevation given a known distanc
and the base level, and an evaluated slope. The Hazeva fluvial syste
Mediterranean at an elevation of ~0 m.a.s.l, and over a distanc
Mediterranean coast to the location of exposed chert nodules. Given
of ~0.5%, the elevation of the Central Jordanian Plateau is ~1 km
different types of evidence reported, it is reasonable to presume tha
Arabian Peninsula reached its current elevation (~1 km) during the ear
a single elevation to calculate paleo-production rates introduces a seco
account for spatial variations in elevation due to catchment topogra

the two silicate members, concentrations (and exposure times) of the sa
or higher than the chert samples (Fig. 3). This observation agrees with
cosmogenic ^{21}Ne measured in the Miocene chert pebbles represents
during exhumation from bedrock coupled with transport in the Hazev
300 the sand samples have undergone previous sedimentary cycles and co
^{21}Ne. Therefore, sand samples cannot be used to calculate the time sedi
transport in the Hazeva fluvial system or to infer erosion rates. Unlike
feasibly undergone previous exhumation, erosion, and deposition, the M
not undergone previous sedimentary cycles. Hence, all cosmogenic ^{21}
305 during erosion and transport in the Hazeva River and rates of surface pr
can be evaluated using the Miocene chert samples.

The cosmogenic ^{21}Ne exposure times calculated from the Jordanian
269±63 to 378±76 kyr. Exposure times that were calculated from ^{10}
measured in sample EJC5 overlap within uncertainty with ^{21}Ne calcula
310 2). In contrast, exposure times calculated from ^{10}Be and ^{26}Al concent
EJC3 are much shorter ~13-16 kyr, an order of magnitude difference
this discrepancy, we believe that the representative results are longer
^{21}Ne calculated exposure time in sample EJC3 agrees with the ^{21}Ne
exposure times for sample EJC5. Secondly, the timescales of exposur
315 in eroding surfaces at hyperarid Negev Desert are similar and range
(Boroda et al., 2014; Fruchter et al., 2011; Matmon et al., 2009). We c
in modern Jordanian Central Plateau chert nodules range ~300-400 kyr

sites and different depths, so it is unlikely that they all represent the
consider the range of times obtained from Miocene samples to be a good
surface processes.

5.3 Modern and Miocene Erosion Rates and the Influence of Clim

The calculated exposure times of the Jordanian chert nodules are equiv
12 mm/kyr (Table 2), consistent with other rates measured in the regio
2017 and references therein). Calculation of paleo-erosion rates is
Miocene cherts were sampled post-deposition and represent exposur
bedrock and transport in the Hazeva River. However, Miocene expos
or overlap within uncertainty with times of *in situ* Jordanian chert. Th
rates during the Miocene must have been faster than the prevailing rat
While we cannot determine how much faster paleo-erosion rates wer
increase in erosion rates in a hyperarid desert must be the consequence
conditions that prevailed in the region at that time. An increase i
commonly attributed to perturbations in fluvial basins in response
warmer/wetter climatic conditions (e.g., DiBiase and Whipple, 2011; R
and Ehlers, 2006; Val et al., 2016; Willenbring et al., 2013). For exam
brings about higher river discharge and enhancement of the stream p
erosion and sediment transport. Erosion rates in fluvial systems al
induced changes in base level that increase slope steepness and inst
stream power and more sediment readily available for transport. Here

exhumation rates during the mid-Miocene (~18 Myr; Morag et al.
topographic changes could still drive large-scale landscape response
erosion rates and the establishment of the Hazeva fluvial system.

In addition to tectonic forcing, there is ample evidence for a warme
region during the Miocene. Locally, the appearance of mammals in the
and grassy vegetation during the early-mid Miocene, supports a hum
et al., 1988; Horowitz, 2002; Tchernov et al., 1987). Tropical to subtr
the eastern Arabian Peninsula, as indicated by fossilized mangrove roo
1980). Locally, Kolodny et al. (2009), interpreted the ^{18}O in lacustrin
part of the Hazeva unit to be deposited by ^{18}O-depleted paleo-meteori
the presence of a warm ocean to the southeast of the region during
Miocene resulted in tropical cyclones being more prevalent and increa
Together, the above observations suggest climatic conditions that coul
are faster than observed rates in hyperarid conditions, and that support
maintained fluvial system, such as the Hazeva River, during the Mioc

6. Conclusions

We compared the cosmogenic ^{21}Ne measured in chert pebbles an
transported during the mid-Miocene (~18 Myr) by the Hazeva River
(Eocene chert nodules) currently eroding in the Central Jordanian Plat
We successfully established a novel application for measuring cosmo
Miocene chert samples, expanding the opportunities and settings in

Plateau. While it is impossible to determine the exact rate of erosi
cosmogenic ^{21}Ne was produced during erosion from the bedrock and t
exposure times during the Miocene point to rates of surface erosion
390 increased rates during the early-mid Miocene cannot be easily const
climatic conditions. The entire region experienced tectonic uplift a
possibly decreasing during the mid-Miocene, brought on topographic
Hazeva fluvial system and could have manifested as faster rates of su
multiple independent proxies presented in previous studies support w
395 the region during the early-mid Miocene. Increased precipitation woul
bedrock erosion deduced as well as the higher water discharge needed
the Hazeva River. Finally, the variability observed in exposure times
might represent a change in rates of erosion throughout the Miocene.
^{21}Ne concentrations is more likely the result of fluvial transport dynam
400 exposure during transport in this large Miocene river.

Data availability

A raw data table, including all Ne isotope measurements, and three-iso

the supplement.

Author contribution

405 MBI and AM designed the study. MBI collected the samples for analys

This work was funded by the Israel Science Foundation (*ISF* grant n
further supported by the United States-Israel Binational Science Foun
2017229 to MBI). We greatly appreciate the intensive work and ins
Taylor Schildgen, Dr. Marissa Tremblay, and an anonymous reviewer
O. Tirosh, and Y. Burstyn for laboratory and field assistance. MBI woul
and administrative staff at the Berkeley Geochronology Center for th
This work was performed in part under the auspices of the U.S. Departm
Livermore National Laboratory, United States under Contract DE-A
LLNL-JRNL-788357.

References

Allen, P. A.: From landscapes into geological history, Nature, 451(71
doi:10.1038/nature06586, 2008.

Anderson, R. S., Repka, J. L. and Dick, G. S.: Explicit treatment of inh
depositional surfaces using in situ 10Be and 26Al, Geology, 24(1), 47,
7613(1996)024<0047:ETOIID>2.3.CO;2, 1996.

Avni, Y., Bartov, Y., Ginat, H. and Ginata, H.: The Arava Formation-
Arava Valley and its western margin, southern Israel, Isr. J. Earth Sci.
doi:10.1092/5U6A-RM5E-M8E3-QXM7, 2001.

Avni, Y., Segev, A. and Ginat, H.: Oligocene regional denudation of t
Pre- and syn-breakup stages of the Afro-Arabian plate, Bull. Geol. Soc
1897, doi:10.1130/B30634.1, 2012.

base level in the early middle Miocene as inferred from geomorpholog
western fluvial outlet, Geomorphology, 261, 147–161, doi:10.1016/j.g
2016.
Ben-Israel, M., Matmon, A., Haviv, I. and Niedermann, S.: Applying s
understand surface processes in deep geological time (10^7–10^8yr),
498, 266–274, doi:10.1016/j.epsl.2018.07.002, 2018.
Bierman, P. R.: Using in situ produced cosmogenic isotopes to estima
evolution: A review from the geomorphic perspective, J. Geophys. Re
doi:10.1029/94JB00459, 1994.
Bierman, P. R. and Caffee, M.: Slow Rates of Rock Surface Erosion a
across the Namib Desert and Escarpment, Southern Africa, Am. J. Sci
doi:10.2475/ajs.301.4-5.326, 2001.
von Blanckenburg, F.: The control mechanisms of erosion and weathe
cosmogenic nuclides in river sediment, Earth Planet. Sci. Lett., 237(3-
doi:10.1016/j.epsl.2005.06.030, 2005.
Bohannon, R. G., Naeser, C. W., Schmidt, D. L. and Zimmermann, R.
volcanism, and rifting peripheral to the Red Sea: A case for passive rif
94(B2), 1683, doi:10.1029/JB094iB02p01683, 1989.
Borchers, B., Marrero, S., Balco, G., Caffee, M., Goehring, B., Lifton,
Phillips, F., Schaefer, J. and Stone, J.: Geological calibration of spalla
CRONUS-Earth project, Quat. Geochronol., 31, 188–198, doi:10.1016
2016.

Calvo, R. and Bartov, Y.: Hazeva Group , southern Israel : New obser
implications for its stratigraphy , paleogeography , and tectono-, Isr. J.
475 99, doi:10.1560/B02L-6K04-UFQL-KUE3, 2001.
DiBiase, R. A. and Whipple, K. X.: The influence of erosion threshold
the relationships among topography, climate, and erosion rate, J. Geop
F04036, doi:10.1029/2011JF002095, 2011.
Dunai, T. J.: Cosmogenic Nuclides: Principles, Concepts and Applicat
480 Sciences, edited by Intergovernmental Panel on Climate Change, Cam
Cambridge., 2010.
Dunai, T. J., González López, G. a. and Juez-Larré, J.: Oligocene-Mio
Atacama Desert revealed by exposure dating of erosion-sensitive land
321–324, doi:10.1130/G21184.1, 2005.
485 Feinstein, S., Eyal, M., Kohn, B. P., Steckler, M. S., Ibrahim, K. M., M
Uplift and denudation history of the eastern Dead Sea rift flank, SW Je
apatite fission track thermochronometry, Tectonics, 32(5), 1513–1528
Ferrier, K. L., Huppert, K. L. and Perron, J. T.: Climatic control of bed
Nature, 496(7444), 206–209, doi:10.1038/nature11982, 2013.
490 Fruchter, N., Matmon, A., Avni, Y. and Fink, D.: Revealing sediment
transport during erosional crater evolution in the hyperarid Negev Des
Geomorphology, 134(3–4), 363–377, doi:10.1016/J.GEOMORPH.201
Garfunkel, Z.: Internal structure of the Dead Sea leaky transform (rift)
kinematics, Tectonophysics, 80, 81–108, doi:10.1016/0040-1951(81)9

2006.

Granger, D. E. and Muzikar, P. F.: Dating sediment burial with in situ
nuclides: theory, techniques, and limitations, Earth Planet. Sci. Lett., 1
doi:10.1016/S0012-821X(01)00309-0, 2001.

Guralnik, B., Matmon, A., Avni, Y., Porat, N. and Fink, D.: Constrain
terraces with integrated OSL and cosmogenic nuclide data, Quat. Geo
doi:10.1016/J.QUAGEO.2010.06.002, 2011.

Hetzel, R., Niedermann, S., Ivy-Ochs, S., Kubik, P. W., Tao, M. and G
and 26Al exposure ages of fluvial terraces: the influence of crustal Ne
Sci. Lett., 201(3–4), 575–591, doi:10.1016/S0012-821X(02)00748-3,

Horowitz, A.: Elephants, horses, humans, and others: Paleoenvironme
bridge, Isr. J. Earth Sci., 51(3–4), 203–209, doi:10.1560/YTDR-LW6I

Ivy-Ochs, S. and Kober, F.: Surface exposure dating with cosmogenic
179–209, doi:10.3285/eg.57.1-2.7, 2008.

Kohl, C. P. and Nishiizumi, K.: Chemical isolation of quartz for measu
produced cosmogenic nuclides, Geochim. Cosmochim. Acta, 56(9), 3
doi:10.1016/0016-7037(92)90401-4, 1992.

Kolodner, K., Avigad, D., Ireland, T. R. and Garfunkel, Z.: Origin of l
sandstones of North-east Africa and arabia from detrital zircon U-Pb S
Sedimentology, 56(7), 2010–2023, doi:10.1111/j.1365-3091.2009.010

Kolodny, Y.: The lithostratigraphy and petrology of the Mishash chert
University, Jerusalem., 1965.

chronology and production rate cross-calibration of five cosmogenic n
systems from the southern Central Andean Plateau, Earth Planet. Sci.
doi:10.1016/j.epsl.2018.07.034, 2018.
Matmon, A. and Zilberman, E.: Landscape Evolution along the Dead
in Quaternary of the Levant, edited by Y. Enzel and O. Bar-Yosef, pp.
University Press., 2017.
Matmon, A., Simhai, O., Amit, R., Haviv, I., Porat, N., McDonald, E.,
R.: Desert pavement-coated surfaces in extreme deserts present the lon
Earth, Geol. Soc. Am. Bull., 121(5–6), 688–697, doi:10.1130/B26422
McFadden, L. D., Eppes, M. C., Gillespie, A. R. and Hallet, B.: Physic
landscapes due to diurnal variation in the direction of solar heating, Ge
117(1), 161, doi:10.1130/B25508.1, 2005.
Meulenkamp, J. E. and Sissingh, W.: Tertiary palaeogeography and te
evolution of the Northern and Southern Peri-Tethys platforms and the
the African–Eurasian convergent plate boundary zone, Palaeogeogr. P
196(1–2), 209–228, doi:10.1016/S0031-0182(03)00319-5, 2003.
Morag, N., Haviv, I., Eyal, M., Kohn, B. P. and Feinstein, S.: Early fla
Rift: Implications for the role of mantle plumes and the onset of the D
Planet. Sci. Lett., 516, 56–65, doi:10.1016/j.epsl.2019.03.002, 2019.
Omar, G. I. and Steckler, M. S.: Fission Track Evidence on the Initial
Two Pulses, No Propagation, Science (80-.)., 270(5240), 1341–1344,
doi:10.1126/science.270.5240.1341, 1995.

doi:10.1016/j.epsl.2006.05.027, 2006.

Schaller, M., Von Blanckenburg, F., Veldkamp, A., Tebbens, L. A., H
W.: A 30 000 yr record of erosion rates from cosmogenic 10Be in Mid
terraces, Earth Planet. Sci. Lett., 204(1–2), 307–320, 2002.

Shuster, D. L. and Farley, K. A.: Diffusion kinetics of proton-induced
quartz, Geochim. Cosmochim. Acta, 69(9), 2349–2359, doi:10.1016/j.

Sinclair, H. D., Stuart, F. M., Mudd, S. M., McCann, L. and Tao, Z.: D
records decoupling of source-to-sink signals by sediment storage and r
present rivers of the Great Plains, Nebraska, USA, Geology, 47(1), 3–
2019.

Tchernov, E., Ginsburg, L., Tassy, P. and Goldsmith, N. F.: Miocene r
(Israel), J. Vertebr. Paleontol., 7(3), 284–310, doi:10.1080/02724634.1

Tremblay, M. M., Shuster, D. L. and Balco, G.: Diffusion kinetics of 3
and implications for cosmogenic noble gas paleothermometry, Geochi
186–204, doi:10.1016/j.gca.2014.08.010, 2014.

Val, P., Hoke, G. D., Fosdick, J. C. and Wittmann, H.: Reconciling tec
sedimentation and spatial patterns of erosion from 10Be paleo-erosion
Precordillera, Earth Planet. Sci. Lett., 450, 173–185, doi:10.1016/j.eps

Vance, D., Bickle, M., Ivy-Ochs, S. and Kubik, P. W.: Erosion and ex
from cosmogenic isotope inventories of river sediments, Earth Planet.
288, doi:10.1016/S0012-821X(02)01102-0, 2003.

Whipple, K. X.: The influence of climate on the tectonic evolution of

Wilson, J. W. P., Roberts, G. G., Hoggard, M. J. and White, N. J.: Cen
Arabian Peninsula from drainage modeling, Geochemistry, Geophys.
3761, doi:10.1002/2014GC005283, 2014.

Zilberman, E. and Calvo, R.: Remnants of Miocene fluvial sediments
and the Jordanian Plateau: Evidence for an extensive subsiding basin i
margins of the Arabian plate, J. African Earth Sci., 82, 33–53,
doi:10.1016/j.jafrearsci.2013.02.006, 2013.

605

Table 1: Sample Description, Sampling Site Locations and Cosmogenic Nuc

Sample	Sample type	Site	Sampling depth below surface (m)	Location		Elevation (m.a.s.l)	Be Carrier (mg)	$^{10}Be/^{9}Be$ ($\times10^{-13}$)	[^{10}Be] (10^5 atoms/ g SiO_2)
				Lat (°N)	Long (°E)				
MHS1	Quartz sand	Paran Valley, Israel	30	30.33296	34.92724	290	176	0.17±0.03	0.14±0.02
MHS3	Quartz sand	Arad Quarry, Israel	90	31.23372	35.20685	570	171	0.36±0.02	0.29±0.02
MHS5	Quartz sand	Arad Quarry, Israel	100	31.23372	35.20685	570	175	0.32±0.02	0.26±0.02
MHC2	Chert pebble	Paran Valley, Israel	20	30.33296	34.92724	290	NA	NA	NA
MHC3	Chert pebble	Arad Quarry, Israel	90	31.23372	35.20685	570	NA	NA	NA
MHC5a	Chert pebble	Arad Quarry, Israel	100	31.23372	35.20685	570	NA	NA	NA
MHC5b	Chert pebble	Arad Quarry, Israel	100	31.23372	35.20685	570	172	NA	NA
MHC6	Chert pebble	Paran Valley, Israel	30	30.33296	34.92724	290	170	0.10±0.01	0.39±0.03
EJC3	In situ chert	Central Jordanian Plateau	Surface	30.97045	36.64469	910	172	0.70±0.03	1.13±0.05
EJC5	In situ chert	Central Jordanian Plateau	Surface	30.87181	36.52129	1000	178	18.43±0.30	29.75±0.49

Note: NA – not available. Samples were either not analyzed, or no result was attained.

*Measurement uncertainties are ~5%.

†Cosmogenic ^{21}Ne is the excess of ^{21}Ne concentrations relative to the atmospheric $^{21}Ne/^{20}Ne$ ratio, calculated for the low-temperature steps (<

Table 2: Exposure times and erosion rates calculated for the modern and Miocene samples

Sample	Sample type	Location	Exposure time (kyr)	Erosion r (mm/kyr
MHS1	Miocene quartz sand	Paran Valley, Southern Negev Desert	114±46 – 166±87	-
MHS3	Miocene quartz sand	Arad Quarry, Northeastern Negev Desert	280±10 – 408±63	-
MHS5	Miocene quartz sand	Arad Quarry, Northeastern Negev Desert	278±17 – 404±83	-
MHC3	Miocene chert pebble	Arad Quarry, Northeastern Negev Desert	167±53 – 242±113	3.0±1.4 -
MHC5a	Miocene chert pebble	Arad Quarry, Northeastern Negev Desert	91±46 – 132±78	5.5±3.3 -
MHC5b	Miocene chert pebble	Arad Quarry, Northeastern Negev Desert	0^{+59}_{-0} – 0^{+85}_{-0}	>8.6 – >
MHC6	Miocene chert pebble	Paran Valley, Southern Negev Desert	121±59 – 176±102	3.0±1.4 -
EJC3*	In situ chert nodule	Central Jordanian Plateau	269±49 / 16±1 / 13±1	2.7±0.5 /
EJC5*	In situ chert nodule	Central Jordanian Plateau	378±76 / 361±6 / 378±3	1.9±0.4 /

Note: Exposure times is the 'simple exposure time' calculated for exposure at the surface, calculated cosmogenic ^{21}Ne production rates rangi yr), given an elevation of 500 and 1000 meters above sea level. Erosion rates for sand samples were not calculated as the concentration of cos inherited cosmogenic ^{21}Ne from previous sedimentary cycles.

*Erosion rates calculated using ^{21}Ne / ^{10}Be / ^{26}Al.

610

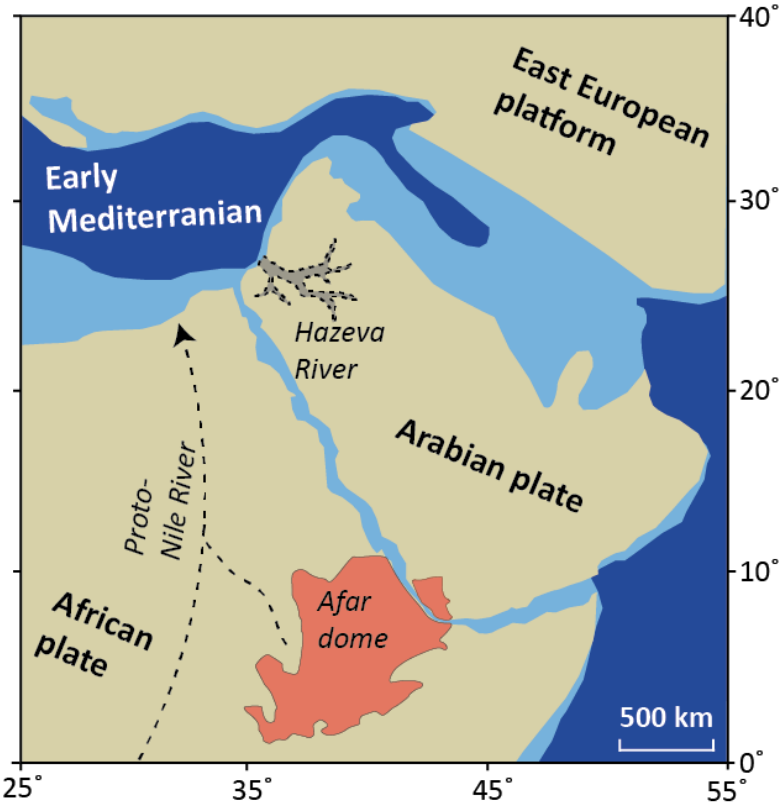

Figure 1. Paleo-geographic map of the eastern Levant during the ear Meulenkamp and Sissingh, 2003) with the approximated extent of the E on Avni et al., 2012; Zilberman and Calvo, 2013).

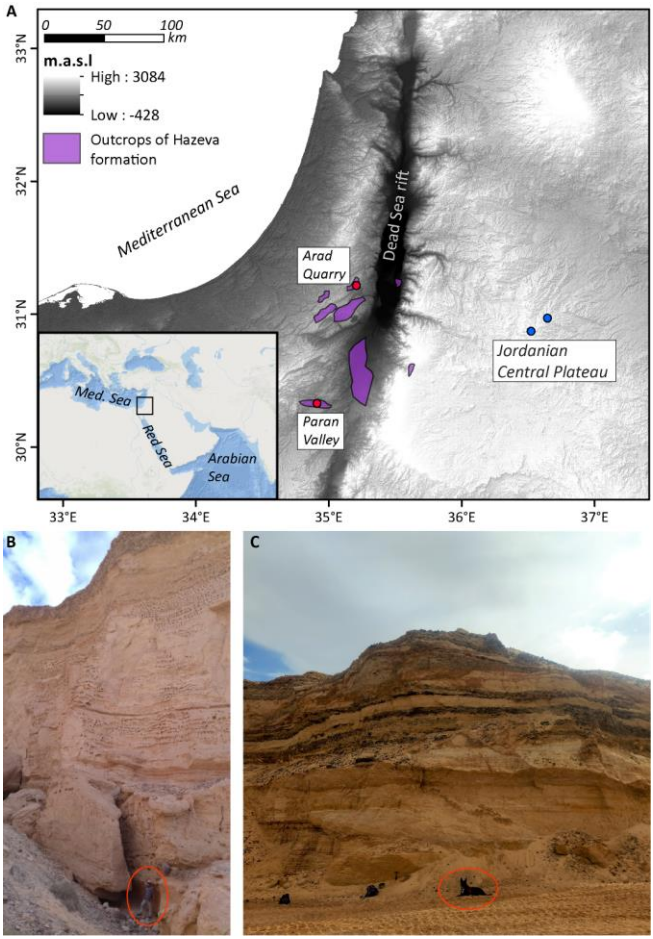

Figure 2. (A) Shaded relief map of the study area with sampling lo sediments (red) and in situ Eocene source rock (blue). Hazeva outcrop Calvo (2013). The inset map shows the regional geographical context. (B) Valley. Sample collected from behind the fallen boulder in a narrow overburden of ~50 meters of sand and conglomerate. See person for scal Photo of sampling location at Arad Quarry. Samples collected from un ~100 meters of quartz sand. See dog for scale marked at the bottom.

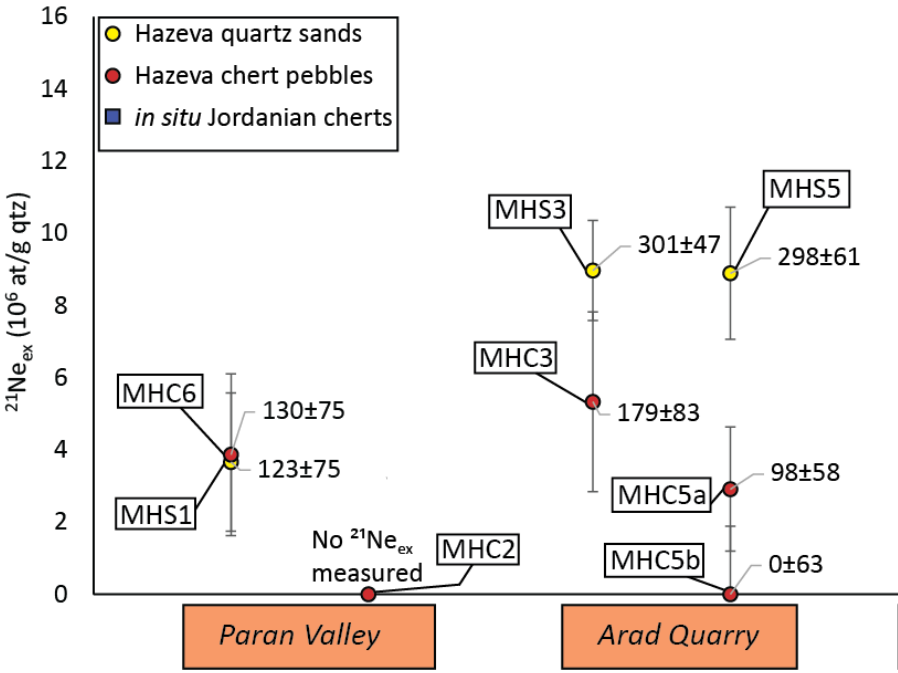

Figure 3. $^{21}Ne_{cos}$ concentrations in Hazeva sands (yellow), Hazeva che
Jordanian Central Plateau chert nodules (blue) with respective uncerta
sample location.

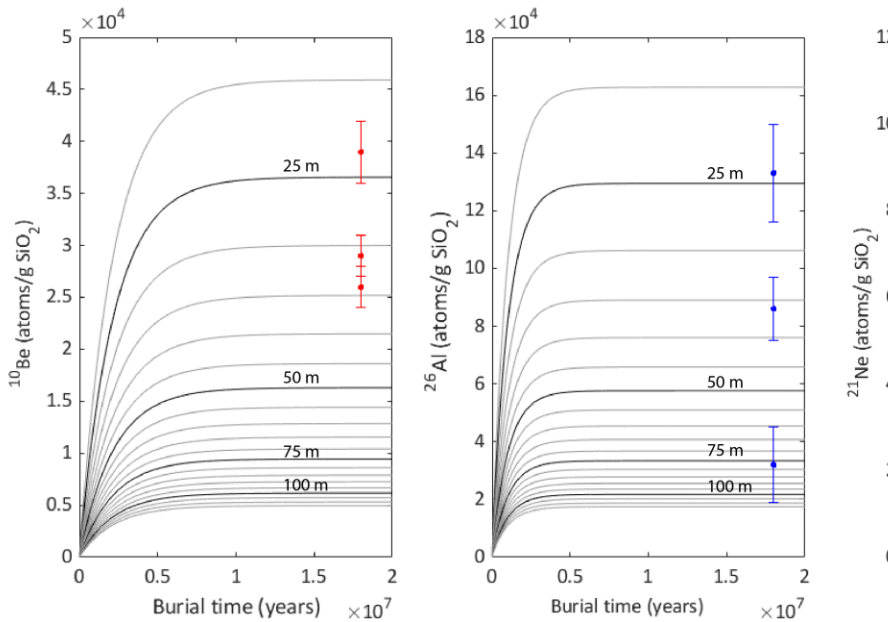

Figure 4. Measured concentrations of ^{10}Be (red), ^{26}Al (blue), and ^{21}Ne
630 **MHS5, and MHC6. Grey contour lines show changes in nuclide concentr**
depths from 20 to 120 m below the surface in 5m increments. For both
sample, the concentrations of cosmogenic ^{21}Ne are higher than the estim
Production by cosmic-ray muons is calculated with schematics presented
rates were calculated at the Arad Quarry site by cosmic-ray muons of
635 **(2017) and of ^{21}Ne by fast muons is after Balco et al. (2019). This illustra**
concentrations can be explained by post-burial production, but ^{21}Ne
significant fraction of cosmogenic ^{21}Ne is pre-burial.